(Received 28 September 2025, Accepted 24 November 2025, Scheduled 10 December 2025)

Compact Multiband Antenna for Implantable Medical Device Applications

Vivek Gupta[1, 2, *] and Rajeev Kumar[2]

[1] University School of Engineering & Technology, Rayat Bahra University, Mohali, Punjab, India
[2] Chitkara University Institute of Engineering & Technology, Chitkara University, Punjab, India

ABSTRACT: This article presents the design and simulation of a small, high-gain circular patch antenna specifically for an implantable biotelemetry application. The antenna is constructed on a Rogers RT/Duroid 6010/6010LM™ substrate, 1.27 mm in thickness, including 0.035 mm circular radiating patches, as well as a ground plane. The antenna is tiny, with a patch radius of 14 mm, and the total volume of the antenna is 825 mm^3. The reduced size creates a more efficient radiation pattern, and the substrate material is high in dielectric constant ($\varepsilon_r = 10.2$), allowing for a smaller size without sacrificing performance. Our suggested work introduces a novel solution to the given problems and presents a compact multi-band implantable antenna for implantable medical devices, which are used in the wireless medical telemetry service (WMTS) (1395–1400 MHz), medical body area network (MBAN) (2360–2400 MHz), lower ultra-wide band (UWB-L) (3100–4800 MHz), and upper ultra-wide band (UWB-U) (4800–10600 MHz) frequency bands. The proposed antenna design intends to enhance bandwidth, efficiency, and radiation pattern, all while remaining within strict size limits and biocompatibility requirements of implantable medical devices by carrying out widespread simulation and experimental verification.

1. INTRODUCTION

Single-band antennas are inappropriate for addressing the demands of multitasking implantable medical devices (IMDs), as these devices necessitate operational frequencies for additional functions, including wake-up and wireless charging, in conjunction with biotelemetry [1]. Multiband implantable antennas for implantable medical devices (IMDs) are therefore in high demand. There is considerable potential for research on multiband implanted antennas for implantable medical devices, while the existing literature in this field is limited. There is significant potential for research on implantable multiband antennas for implantable medical devices, as minimal work has been conducted and documented to date [2–5] in this domain. A dual-band circular patch antenna operating in the Industrial, Scientific, and Medical (ISM) band (2400–2483.5 MHz) and the Medical Implants Communication Service (MICS) band (402–405 MHz) was introduced for biotelemetry applications [2]. Several miniaturization techniques, which involve vias connecting the radiating patch to the ground, were used to produce the antenna's tiny volume of 797.96 mm^3. The suggested antenna achieves a maximum gain of -33.1 dBi at 400 MHz and -14.55 dBi at 2.55 GHz. A dual-band antenna functioning at 402–405 MHz and 2400–2480 MHz with a substantial volume of 642.62 mm^3 was introduced [3]. Apart from its size, this antenna was incompatible with any frequency band that was used for power transfer wirelessly. Additionally, a dual circularly polarized conformal implantable antenna with a volume of 8 mm^3 with frequencies of 402, 915, and 2400 MHz was described [4]. It exhibited circular polarization at frequencies of 915 and 2400 MHz. Because of the loop shape, the antenna had a complex feeding architecture despite its small size, making it impossible to feed in flat settings. An implantable quad-band antenna operates at 405 MHz, 884 MHz, 1449 MHz, and 2638 MHz (MICS, MedRadio, WMTS, ISM), with a volume of 285.75 mm^3 and a gain of -41.1 dBi. An implanted antenna exhibits triple-band functionality, operates at frequencies of 608–614 MHz, 1395–1400 MHz, and 1427–1432 MHz, and has a volume of 536.4 mm^3 in a planar configuration.

The proliferation of "Wireless Body Area Networks (WBANs)" has facilitated the development of implantable antennas for medical devices. The attributes of antennas, including their compact dimensions, lightweight nature, mechanical durability, and flexibility, facilitate their unobtrusive incorporation into implantable medical devices. However, while considering the design of implantable antennas, one must note that these antennas will operate in the ambient environment of the human being. There should also be a regulation in the "Specific Absorption Rate (SAR)", which is the unit used for measuring exposure to electromagnetic radiation with respect to the human body, for ensuring user safety. According to IEEE/ICNIRP/FCC standards, SAR should not exceed an average of 1.6 W/kg per gram of tissue and 2 W/kg per 10 gram of tissue.

Circle-shaped patch antennas have gained enormous interest among several microstrip patch antenna (MPA) designs due to their uniform radiation, small dimensions, and compatibility with various high-frequency applications like satellite communication, radar, and medical devices [6–10]. Copper circular patch antennas have a radiating metallic patch,

* Corresponding author: Vivek Gupta (vivek.gupta@rayatbahrauniversity.edu.in).

a dielectric substrate for structural support, and a conductive ground plane underneath. Substrate affects antenna resonance frequency, bandwidth, and radiation efficiency [11, 12]. Circular patch antennas, with higher polarisation purity and the capability of supporting linear and circular polarisation, are more favourable than rectangular patch antennas in applications demanding polarisation diversity. A circular patch antenna fundamentally operates on the principle of a resonant cavity, where the ground plane and radiating patch constitute a resonator [13, 14]. The TM11 working mode of the circular patch antenna generally exhibits a sinusoidal distribution of the electric field in radial direction [15]. The antenna's resonance frequency is determined only by the patch's height, width, and radius [16]. High-permittivity substrates such as Rogers RT/Duroid 6010/6010LMTM facilitate miniaturization by reducing the physical dimensions required for a specific resonance frequency.

Circular patches fit for space-limited uses as they allow for a smaller footprint than their rectangular equivalents [17]. It is perfect for point-to-point communication; these antennas show a directed radiation pattern with maximal radiation perpendicular to the patch surface [18]. Circular patches naturally show lower cross-polarization than rectangular patches, therefore lowering interference in communication systems [20, 21].

Because of their smaller footprint than rectangular patches [17], circular patches can find application in implantable medical device (IMD). These antennas act safely for point-to-point operation, having a very directed radiation pattern with the maximum radiation emitted normal to the patch surface [18]. Because circular patches will possess lower cross-polarization than their rectangular counterparts, they thereby reduce interference in communication systems [20, 21].

2. RESEARCH METHODOLOGY

The present study adopts a design-oriented experimental methodology to develop a compact multiband circular patch antenna specifically suited for IMD applications. Given the stringent requirements of biomedical antennas — including compactness, functional reliability, and patient safety — the research design integrates theoretical modelling, simulation-based optimisation, and comparative evaluation. The primary focus is on achieving multiband operability across "Wireless Medical Telemetry Service (WMTS)", "Medical Body Area Network (MBAN)", and Ultra-Wideband (UWB) frequency ranges while ensuring compliance with safety regulations that involve "Specific Absorption Rate (SAR)" limits.

3. DESIGN METHODOLOGY

3.1. Design of Multiband Antenna System

A circular radiating patch forms the central element of the antenna, serving as the primary source of electromagnetic wave generation. Its resonant frequency is largely governed by its geometric dimensions, with smaller patches resonating at higher frequencies. By employing a "Rogers RT/Duroid 6010/6010LM™" substrate ($\varepsilon_r = 10.2$), significant miniaturisation of the patch is achieved without sacrificing electrical performance. This makes the design particularly well suited for applications where antenna compactness is of critical importance, such as implantable biomedical systems, satellite communication, and portable radar units.

The patch is excited through a coaxial probe feed, which plays a vital role in ensuring efficient energy transfer. The choice and placement of the feed point directly influence impedance matching, which in turn reduces reflection losses and maximises power delivery to the radiating element. Properly optimised feeding ensures stable resonance, broader bandwidth, and improved return loss characteristics.

The geometry of suggested antenna is seen in Fig. 1, which employs a circular substrate with a circular patch and ground plane. Both substrate and superstrate use Rogers RT/Duroid 6010/6010LM^{TM} ($\varepsilon_r = 10.2$ and $\tan\delta = 0.0023$) with a thickness of 1.27 mm. To design the proposed antenna, we first have to design a circular patch antenna. According to Balanis [22].

$$a_{eff} = \frac{x11}{2\pi f r\sqrt{\varepsilon r}} \tag{1}$$

$$a = \frac{a_{eff}}{\sqrt{\left\{1 + \frac{2h}{\pi\varepsilon_r a_{eff}}\left[\ln\left(\frac{\pi a_{eff}}{2h}\right)\right]\right\}}} \tag{2}$$

where a_{eff} is the effective radius of the patch, a the actual radius of the patch, h is thickness of the substrate, ε_r the permittivity of the substrate, and x_{11} the Bessel function's first order derivative, which is 1.8412.

The resonance frequency of the circular patch is evaluated by formula

$$f_r = \frac{1.8412C}{2\pi a_{eff}\sqrt{\varepsilon_r}} \tag{3}$$

The top view of proposed antenna (Fig. 1) illustrates the integration of several design techniques intended to achieve compactness, multiband operation, and reliable performance in implantable environments. The circular radiating patch forms the primary radiating element. Its geometry supports symmetrical current distribution, thereby reducing cross-polarisation and ensuring stable radiation patterns irrespective of implant orientation. The proposed antenna is developed and simulated in ANSYS HFSS 2024R1.

3.2. Steps of Proposed Multiband Antenna Design

The proposed antenna uses various slots to maximise its performance, and finally polygon patch is used to support its multiband operation. For the design, a circular patch antenna termed as Ant 1 evolves up to final design Ant 6 presented in Fig. 2.

The circular patch plane acts as the primary radiating element of the antenna. Implemented using perfect electric conductor (PEC) in simulations, the patch is assumed to behave as an ideal conductor, thereby eliminating ohmic losses and enabling accurate evaluation of the intrinsic electromagnetic performance. In the second step, Ant 2, small cuts at top and bottom of the patch in a form of T are used. It fine-tunes the input

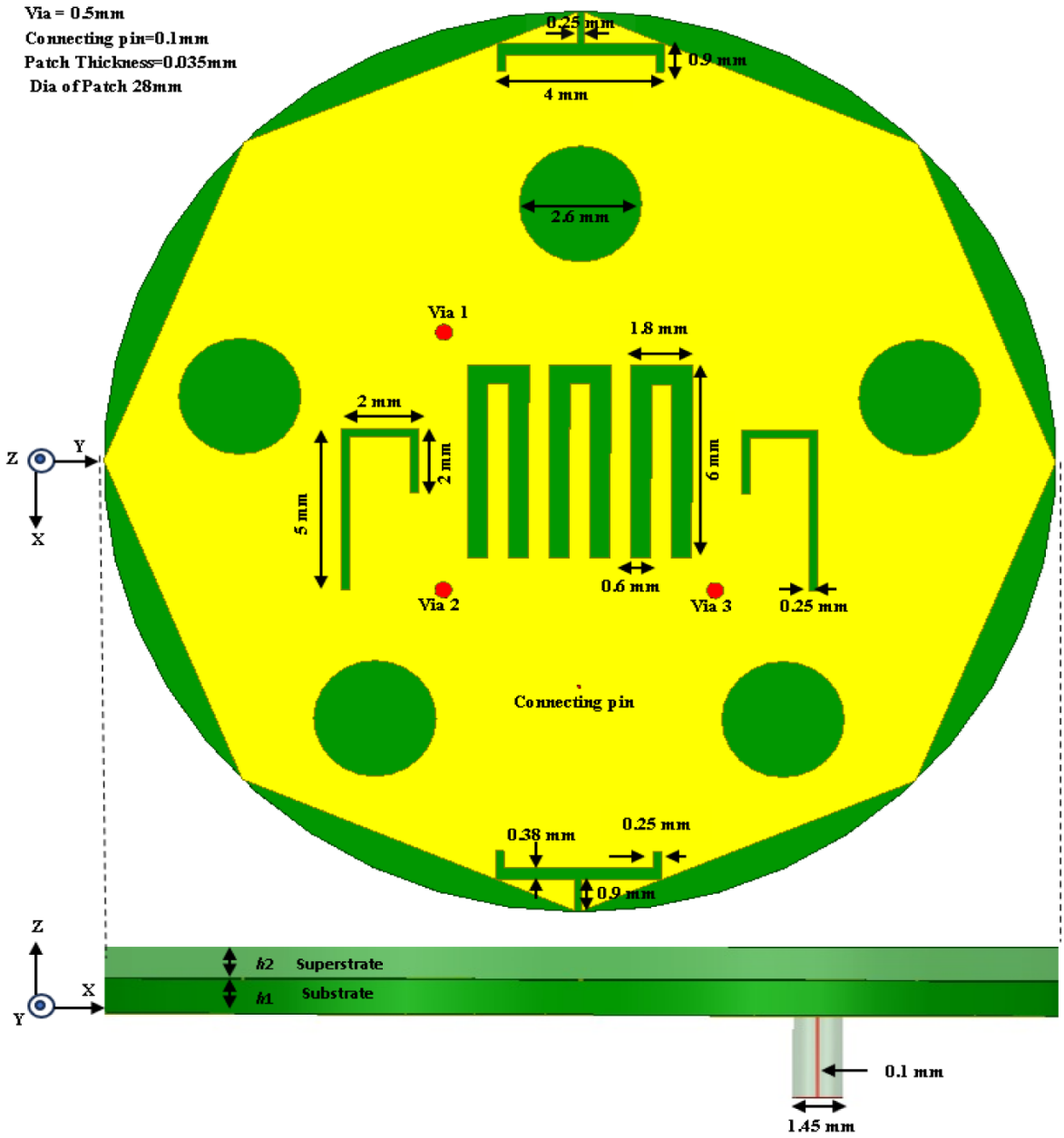

FIGURE 1. Geometry of proposed multiband implantable antenna (unit: mm).

resistance and breaks the modal degeneracy, which reduces the surface current density. It also supports the multiband operation at higher frequencies. There are two more slots surrounding the center in the form of an L that are created. It lengthens surface current path and increases series inductance which helps in match tuning. It also helps in enhancing the bandwidth. The placement of vias has an important role in proposed antenna Ant 3. The via 1 and via 3 are placed diagonally, and together both alter the effective inductance-capacitance network of the radiating patch. It helps in tuning the input impedance, stabilizing resonance, and suppressing parasitic surface modes that can be excited on a high-ε_r substrate. The via 2 forms a quasi-triangular via constellation with via 1 and via 3. This distributed, diagonally balanced placement promotes uniform current return paths and mitigates azimuthal field asymmetries that otherwise increase cross-polarization or distort the main lobe, which is especially useful when the device experiences orientation changes or bending in biomedical settings. The via 2 also helps in confining the fields and reducing backward radiation into tissue, supporting SAR compliance. The three-via arrangement attains deeper S_{11} notches, enhanced band separation, and increased gain stability across all operational bands. Adding more than three vias did not make things much better, and in some cases, it made the design more complicated and harder to make without any real gain. In Ant 4 meander slots are etched at the centre, which increases the electrical-length

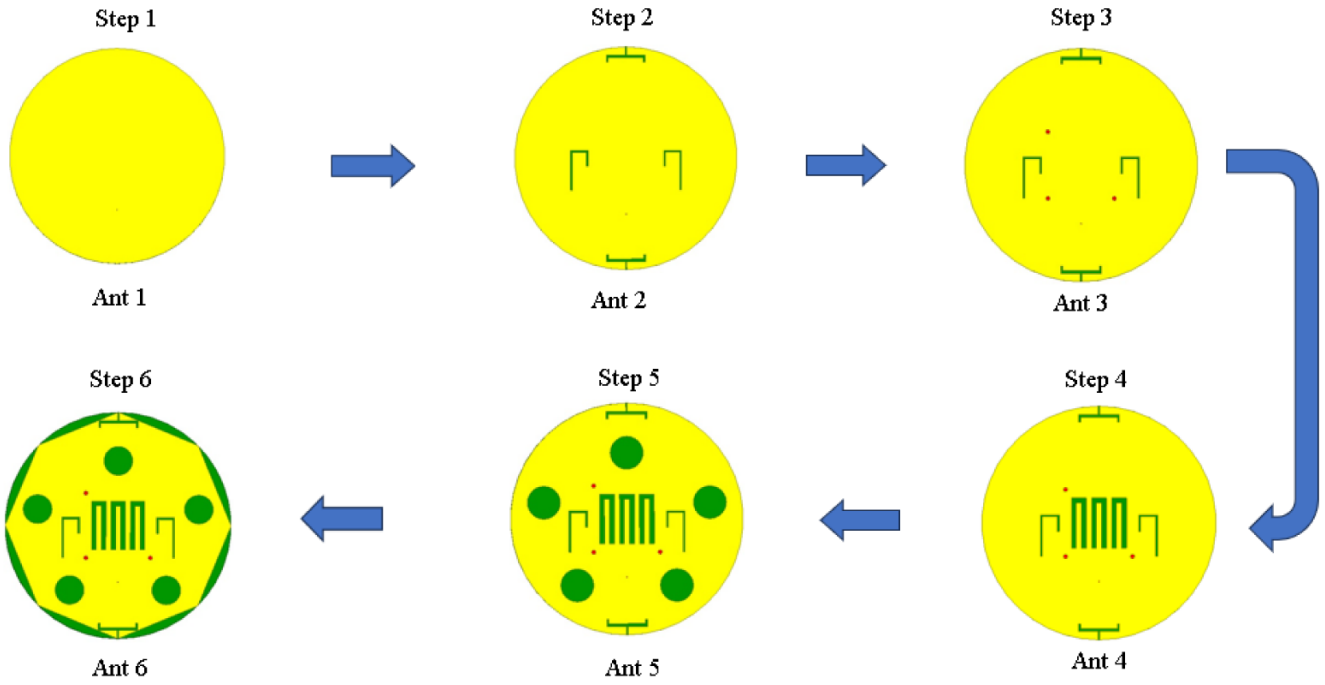

FIGURE 2. Design steps of proposed multiband antenna.

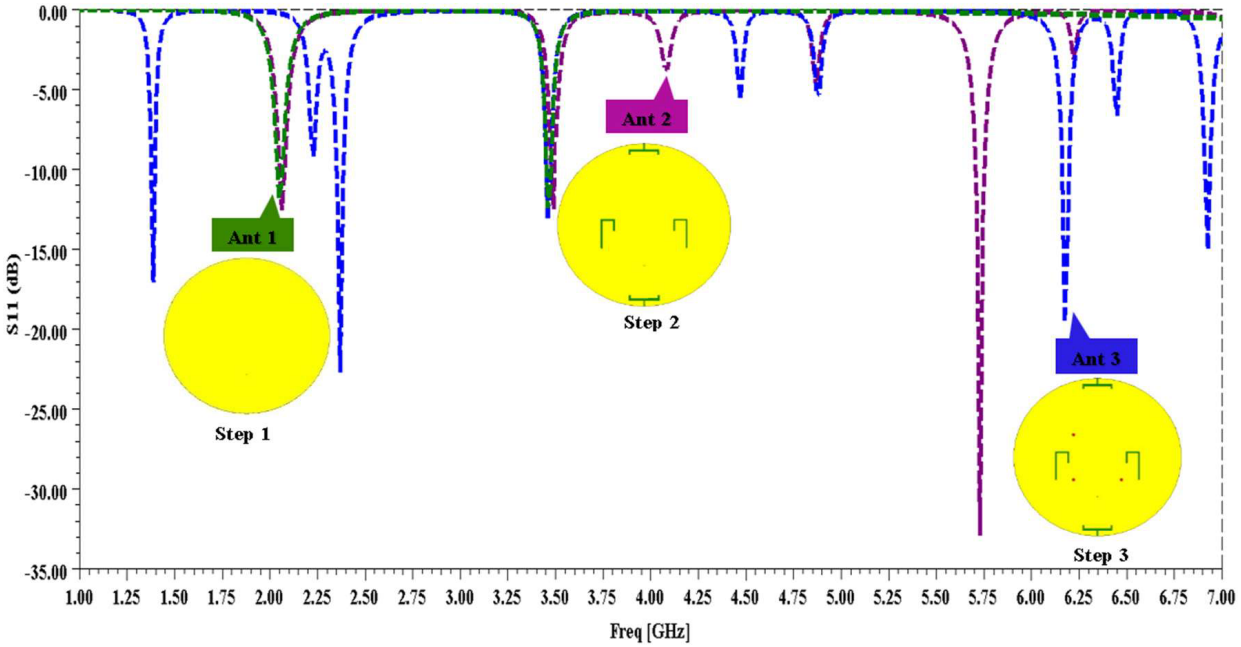

FIGURE 3. Comparison of S_{11} results of Ant 1 to Ant 3.

without footprint growth. The meander slot at the centre of patch enables the lower band by down shifting the one resonance while keeping the original higher band mode. In Ant 5, five circular parasitic slots are etched around the radiator, used to supress the edge current and to improve the bandwidth and efficiency in multiband operation. In Ant 6, a polygon patch is used replacing the circular patch, because polygon patch has advantage to lower the cross polarization and supports more distinct and well separated resonance in multiband operation.

The comparison of S_{11} results of design step of proposed multiband antenna is depicted in Fig. 3 and Fig. 4.

The S_{11} results of design steps of Ant 1 to Ant 6 are shown in Fig. 3 and Fig. 4. Ant 1 has demonstrated itself to be a narrowband baseline, producing two narrow resonances at 2.2 GHz and 3.5 GHz. In the second step of Ant 2, a new mode is produced at 5.74 GHz, with further resonances detected at 2.1 GHz and 3.25 GHz. The supplementary mode signifies that the perturbations are efficacious and exhibit improved alignment. Ant

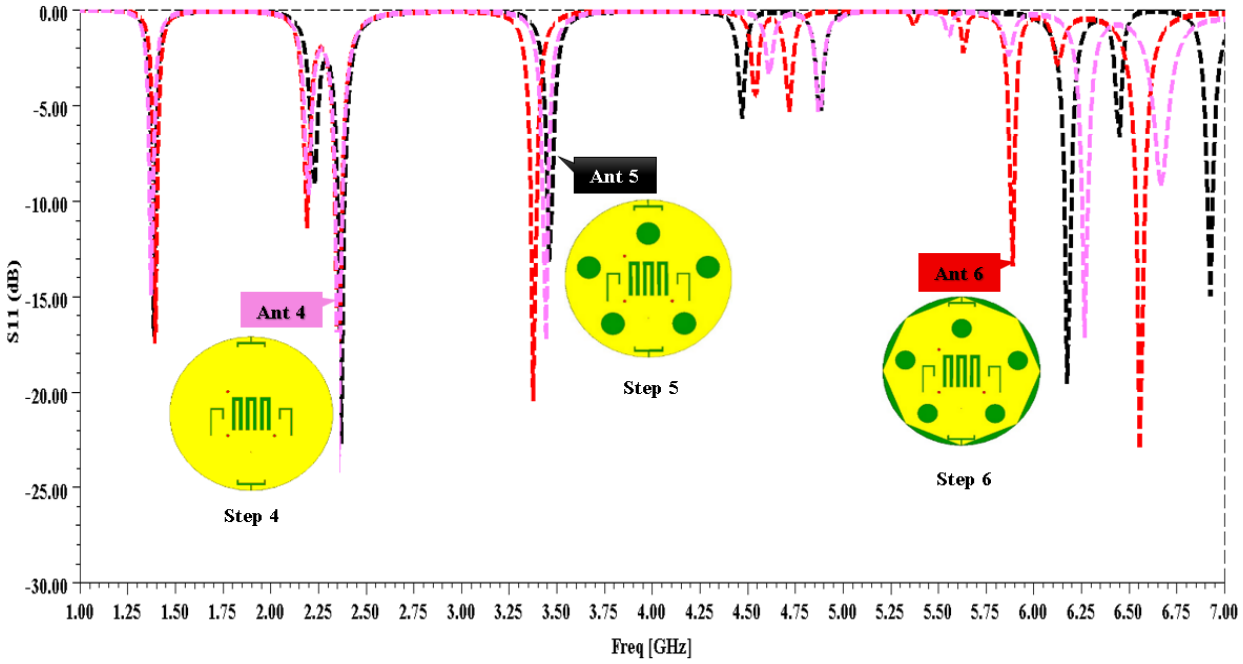

FIGURE 4. Comparison of S_{11} results of Ant 4 to Ant 6.

TABLE 1. Achieved frequency bands with a bandwidth of proposed multiband antenna.

Bands Achieved	Frequency (MHz)	Bandwidth Achieved (MHz)
WMTS	1386–1405	19
MBAN	2336–2374	38
UWB-L	3362–3394	32
UWB-H	6533–6580	47

3 utilizes vias, resulting in the generation of additional modes. The resonance is observed at 1.39 GHz, 2.37 GHz, 3.46 GHz, 6.17 GHz, and 6.92 GHz. It has been observed that higher frequency modes have upshifted beyond UWB-H. In Ant 4, the resonance of all modes is slightly shifted with increased bandwidth. The new resonances have been observed at 1.35 GHz, 2.35 GHz, 3.44 GHz, and 6.26 GHz. It has been observed that in Ant 4 all the modes have much deeper matching, and higher modes require more frequency centring and bandwidth widening. In design step five, Ant 5, the effect of added perturbations increases the number of modes and match depth, but centering is off. It is also observed that low-frequency modes sit below targets, and high-frequency modes are shifted upward. In the last step of design, Ant 6, it is observed that compared with earlier designs, Ant 6 achieved the robust multi-resonance behaviour and excellent matching at all required bands used in implantable biotelemetry. The achieved frequency band and bandwidth are depicted in Table 1.

4. SIMULATION RESULTS

A thorough parametric analysis was conducted via simulations for the proposed design Ant. 6, as illustrated in Fig. 1.

TABLE 2. Obtain SAR and Gain at different layers of skin phantom of proposed antenna.

Layers	SAR W/kg (over 1 g of tissue)	Gain Total (dB)
Skin	0.423	−6.6
Fat	0.318	0.8
Muscle	0.376	−30.9
Skin Phantom	0.352	−31.5

4.1. SAR Analyses for Implantable Safety

A planar three-layered human tissue model measuring 90 mm × 90 mm × 33 mm, comprising skin, fat, and muscle [23], is modelled in High Frequency Structure Simulator (HFSS) as depicted in Fig. 5. The dielectric characteristics of each tissue and their thicknesses are defined in Fig. 5.

The proposed multiband antenna is tested for each layer separately by inserting it into each layer. The SAR is calculated using $SAR = \frac{\sigma}{\rho}|E|2$, where '$E$' (V/m) represents the electric field intensity; 'σ' (S/m) indicates conductivity of human tissue; and 'ρ' (kg/m^3) reflects the mass density of human tissue. The IEEE/ICNIRP/FCC state that 1.6 W/kg for one gram of tissue and 2 W/kg for ten grams of tissue are acceptable SAR values. To determine SAR value, a benchmark input power of one watt was selected. Fig. 6 illustrates the computation of the SAR across multiple layers of one gram of human tissue.

It is possible to acquire an understanding of both safety and performance parameters by referring to Table 2, which presents the findings of the SAR and total gain over the various phantom layers. SAR for the skin layer is 0.423 W/kg, which is within the safety guidelines established by the IEEE and ICNIRP. However, this value is accompanied by a gain of −6.6 dB, in-

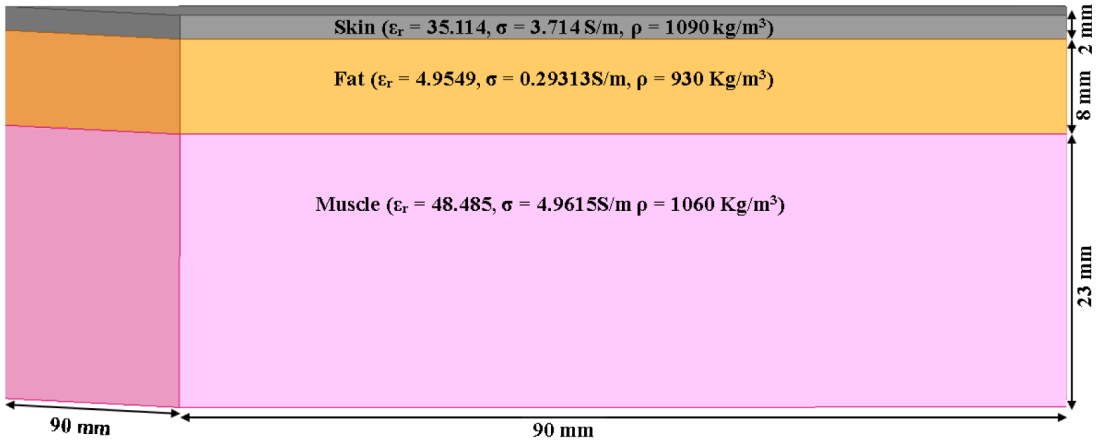

FIGURE 5. Three-layer human skin phantom.

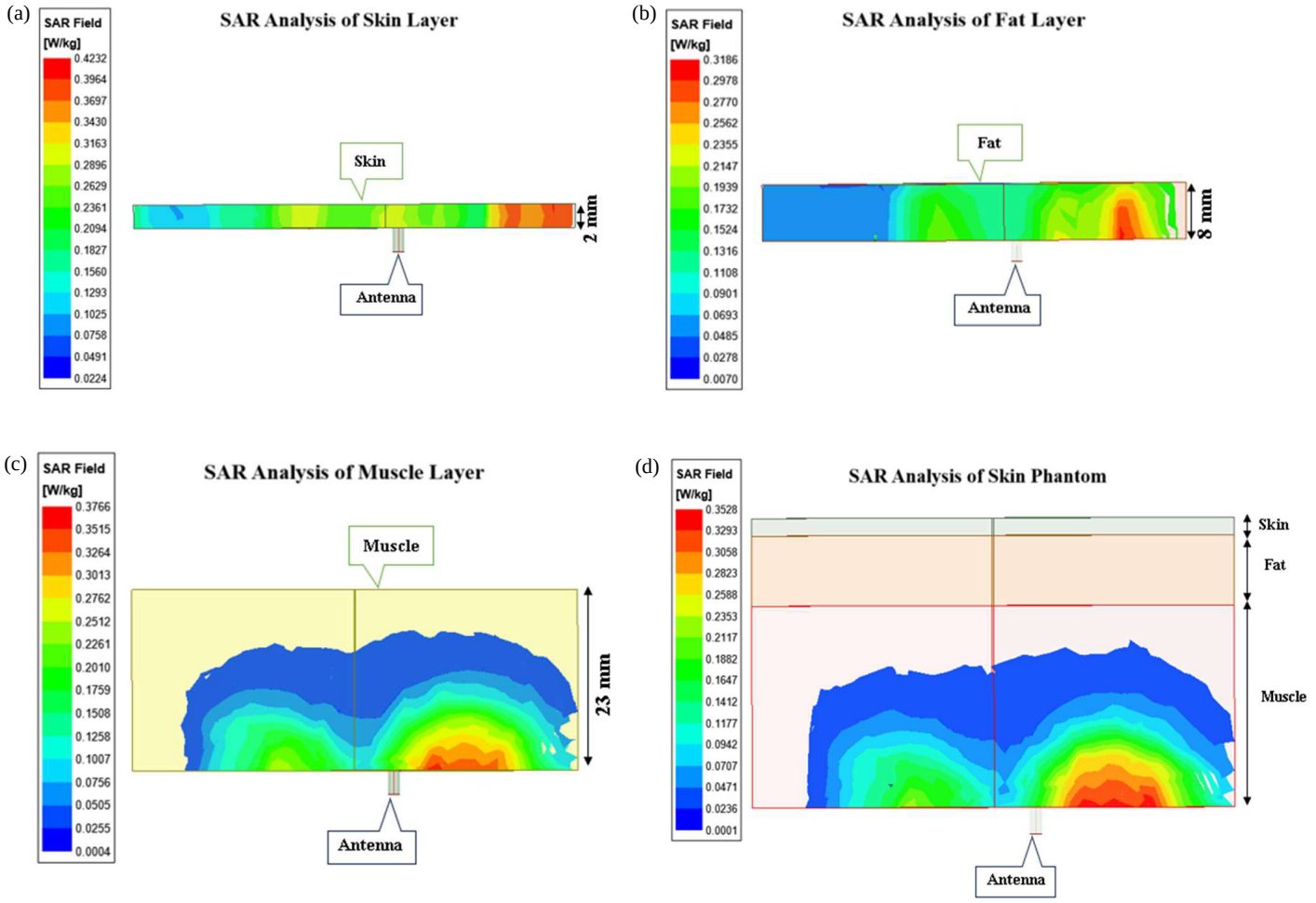

FIGURE 6. Simulated SAR analysis of proposed multiband antenna. (a) Skin layer. (b) Fat layer. (c) Muscle layer. (d) Human skin phantom.

dicating that there is substantial attenuation. SAR drops to 0.318 W/kg in the fat layer, but gain increases to 0.8 dB. This is a significant improvement. As a result of this one-of-a-kind finding, it has been determined that the fat layer is less absorbent and enables enhanced wave propagation, both of which are advantageous for application in biomedical communication systems. Nevertheless, the SAR increases once again to 0.376 W/kg in the muscle layer, but the gain decreases dramatically to −30.9 dB. Muscle layer attenuation is due to its high dielectric constant as well as conductivity.

Although the design is in compliance with SAR safety criteria, the total phantom SAR is reported to be 0.352 W/kg with

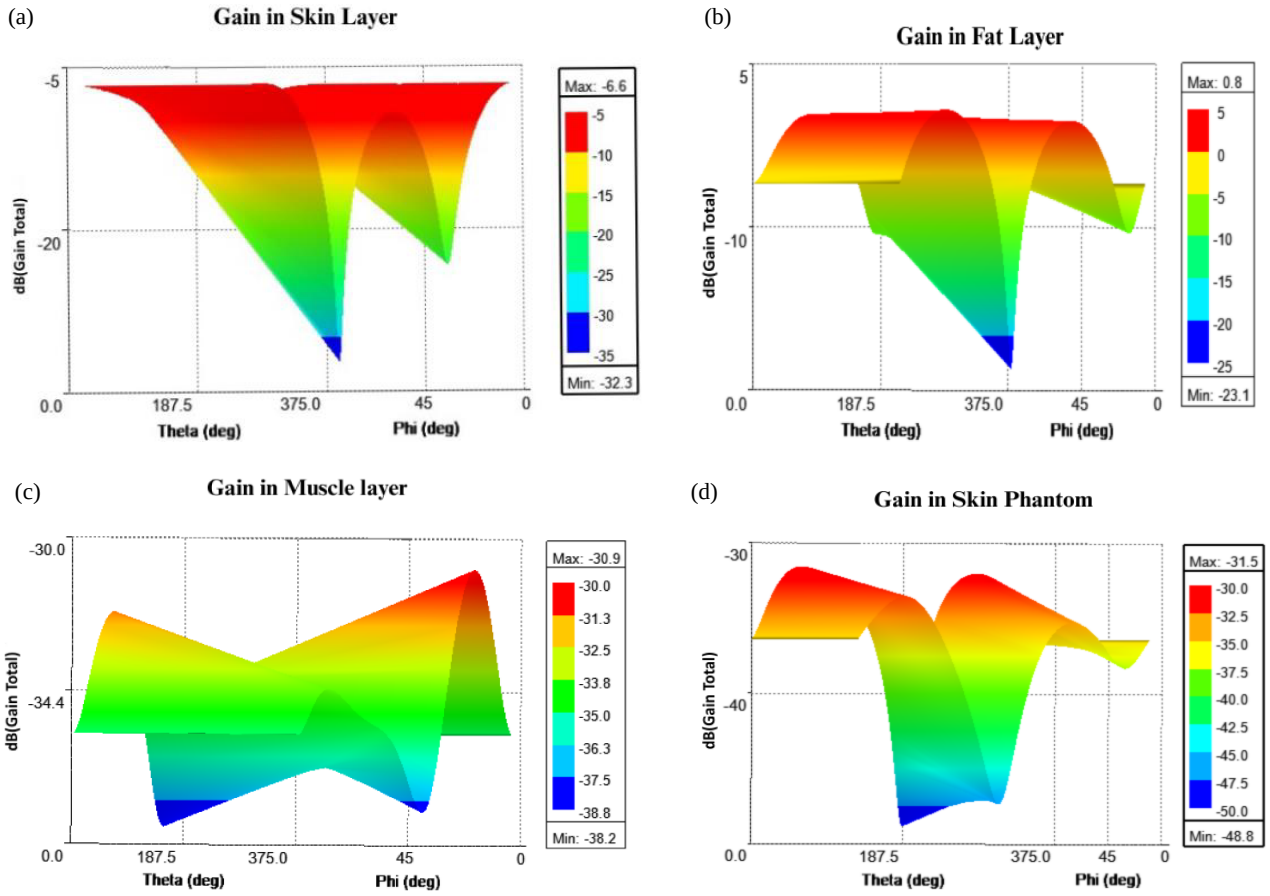

FIGURE 7. Gain of proposed antenna. (a) Skin layer. (b) Fat layer. (c) Muscle layer. (d) Skin phantom.

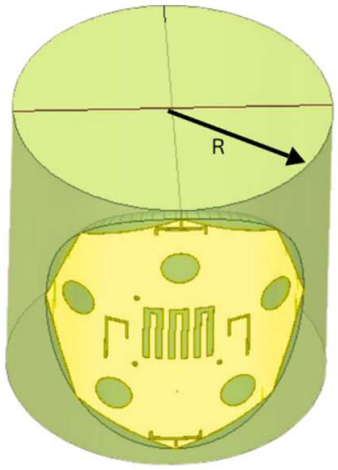

FIGURE 8. Bending of proposed antenna.

a gain of −31.5 dB. This indicates that considerable loss in antenna gain happens in genuine biological contexts. This chart makes it abundantly evident that the combined difficulty of ensuring regulatory compliance (SAR within limitations) while simultaneously attaining acceptable antenna efficiency and gain in tissue-loaded situations is a significant one. Based on these findings, it is clear that although fat layers offer more advantageous propagation, antenna design must take into careful consideration the constraints in performance that are imposed by skin and muscle layers.

4.2. Influence of Bending on Conformal Surface

Given practical implantable contexts, the antenna must conform or bend when being positioned into the user's body, resulting in an unavoidable degree of mismatch. Consequently, it impairs antenna performance, necessitating investigation under various bending conditions. The suggested antenna bends as illustrated in Fig. 8.

An examination of bending at radii of 100 mm, 130 mm, and 160 mm is presented in Fig. 9, which illustrates the impact that mechanical deformation has on the performance of an antenna. Bending affects resonance and bandwidth, particularly at higher frequencies where structural deformation is more likely. Despite this, the antenna is able to retain an acceptable performance at lower frequency bands even when it is bent, which demonstrates both its mechanical durability and flexibility. Because of this, the antenna is appropriate for the use in wearable applications, which need conformal positioning on the body and physical bending that cannot be avoided.

Table 3 examines the frequency and bandwidth response of the proposed antenna, evaluating its mechanical flexibility by testing its performance under various bending radii. The bending radii are 0 mm, 100 mm, 130 mm, and 160 mm. The study demonstrates that bending directly affects impedance matching and resonance characteristics. As curvature intensifies, the bandwidth of the WMTS band progressively decreases, decreasing from 19 MHz at 0 mm to 13 MHz at 160 mm. This signifies that heightened curvature results in a decline in matching

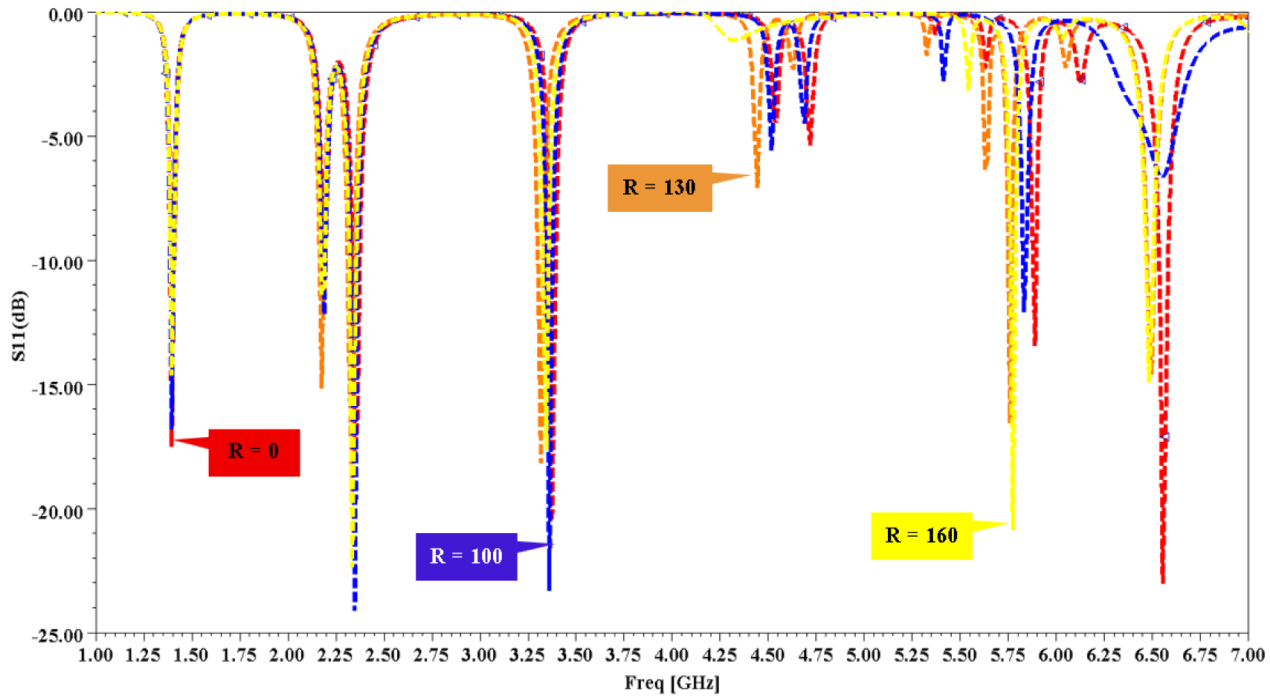

FIGURE 9. Comparison of S_{11} results of bending of proposed antenna.

TABLE 3. Comparison of frequency and bandwidth of proposed antenna over different bending radii.

Radius of bending	$R = 0$ mm		$R = 160$ mm		$R = 130$ mm		$R = 100$ mm	
Frequency Bands	Freq (MHz)	BW (MHz)	Freq (MHz)	BW (MHz)	Freq (MHz)	BW (MHz)	Freq (MHz)	BW (MHz)
WMTS	1386–1405	19	1389–1405	16	1393–1407	14	1388–1401	13
MBAN	2336–2374	38	2320–2356	36	2311–2346	35	2327–2363	36
UWB-L	3362–3394	32	3325–3356	31	3301–3329	28	3346–3377	31
UWB-H	6533–6580	47	6466–6502	36	6471–6506	35	——-	——

within this band. The antenna's durability in this medically pertinent band is underscored by the continuous bandwidth of 35 to 38 MHz inside the MBAN spectrum. Bending causes the bandwidth of the Low UWB to see a minor decrease, going from 32 MHz to 28 MHz. This indicates that the band is somewhat sensitive. In the High UWB, the effect is the most pronounced: when being bent at 0 millimeters, it obtains a bandwidth of 47 millimeters, but when being bent at 160 millimeters, resonance totally disappears, demonstrating that it is susceptible to structural deformation.

Considering the results, it is clear that lower-frequency bands continue to be resistant to mechanical bending, but higher-frequency bands are more likely to experience a decline in performance. Because of this, the antenna is specifically appropriate for the use in WBAN and biomedical monitoring applications, both of which are likely to include bending when it is worn on the bodies of the individuals involved. According to the findings of the investigation, the antenna continues to exhibit satisfactory performance even when being subjected to conformal bending circumstances. This substantiates the antenna's mechanical durability and dependability for the use in wearable healthcare systems.

5. EXPERIMENTAL VALIDATION OF PROPOSED ANTENNA

The proposed antenna is constructed as seen in Fig. 10 and was evaluated for verification. A simple skin-mimicking gel is developed to evaluate the antenna in an implanted environment or in vitro [24].

The skin-like substance contains Triton X-100, sodium chloride, vegetable oil, Gelatine A, hand soap, and deionized water. Coloration is achieved by adding pink food coloring. Every component's electrical qualities were examined, and the results showed that deionized water had the most advantageous electrical characteristics and vegetable oil the least. Changing the quantities of these two components enables the simulation to exhibit both low and high water contents in human soft tissues. Salt can be utilized to make the material more conductive and lower its relative permittivity. Salt induces a rapid decrease in permittivity from 500 MHz to 1 GHz, followed by a more gradual decline from 1 to 20 GHz. Gelatine A, Triton-X, food coloring, as well as hand soap minimally influence the substance's electrical properties due to their composition or their negligible concentration within the mixture. These factors render each hu-

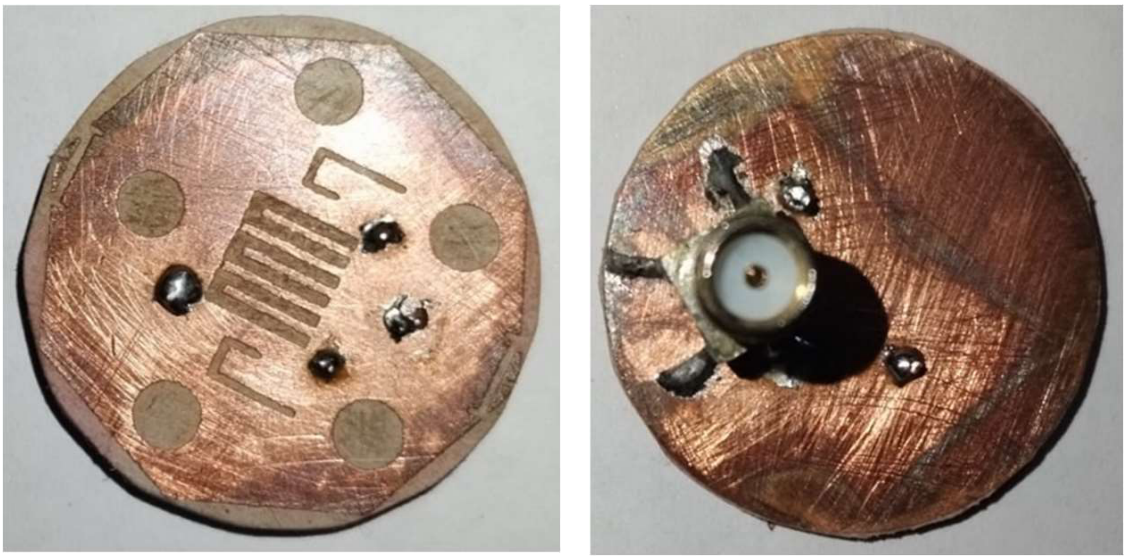

FIGURE 10. Front and back sides of multiband antenna prototype.

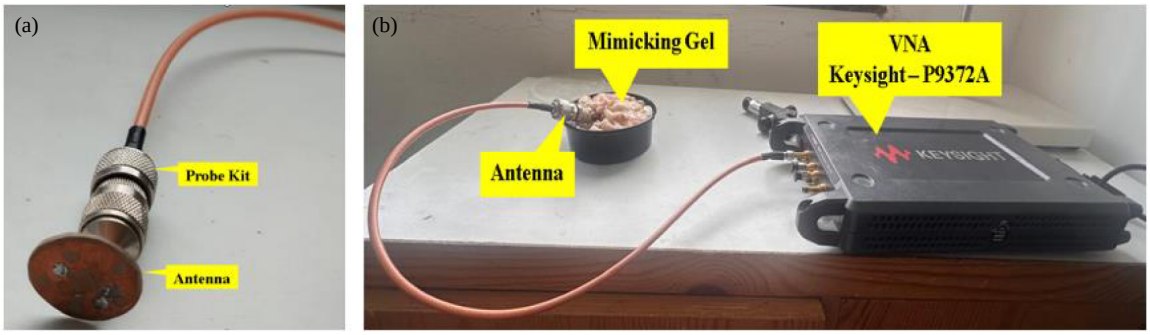

FIGURE 11. Fabricated prototype testing environment using VNA. (a) Free space. (b) Mimicking gel.

TABLE 4. Ingredients for skin-mimicking material.

S. No.	Ingredients	Percent volume
i	Deionised Water	68.33
ii	Vegetable Oil	20.68
iii	Gelatine A	8.99 ($\rho = 1.2\,\mathrm{g\,ml^{-1}}$)
iv	Soap	0.899
v	Triton X-100	0.899
vi	Sodium Chloride	0.166 ($\rho = 2.165\,\mathrm{g\,ml^{-1}}$)
vii	Pink food colouring	0.037 (1 drop = 0.042 ml)

man soft tissue-mimicking substance distinct. Table 4 presents the elements along with their respective percentage quantities.

The antenna's performance is assessed in free space when it is inserted into a skin-mimicking gel solution, as illustrated in Fig. 11.

Figure 12 depicts the S_{11} results for both open space and skin-mimicking gel. A minor difference exists between the measured and simulated outputs, attributable to changes in the antenna's impedance caused by the application of solder for fastening the connecting port and vias.

It is observed that all main resonances are present in both; measured notches are shallower (higher loss, connector/cable radiation) and shift by only a few percent due to fabrication and port de-embedding. Extra ripple in measurement around 4–6 GHz is consistent with feed/fixture parasitic and finite ground effects. In tissue, bands down-shift and narrow versus free space, as expected from higher ε_r and σ.

Figure 13 compares the proposed antenna's gain calculated experimentally and simulated.

The simulated (black dashed) and measured (red dashed) results show several similarities and differences in total gain across the frequency spectrum. Both curves generally have the same overall form, with dips at controlled medical bands and peaks around ultra-wideband frequencies. The observed and simulated findings are very similar at lower frequencies, but they start to differ at certain points, especially near the peaks in the ultra-wideband areas. The measured gain in the WMTS and MBAN regions is always lower than the simulated gain. It means that there are more losses or greater attenuation in real life than what models indicate. The measured curve shows that the nulls (lowest gain points) are deeper and sharper, which

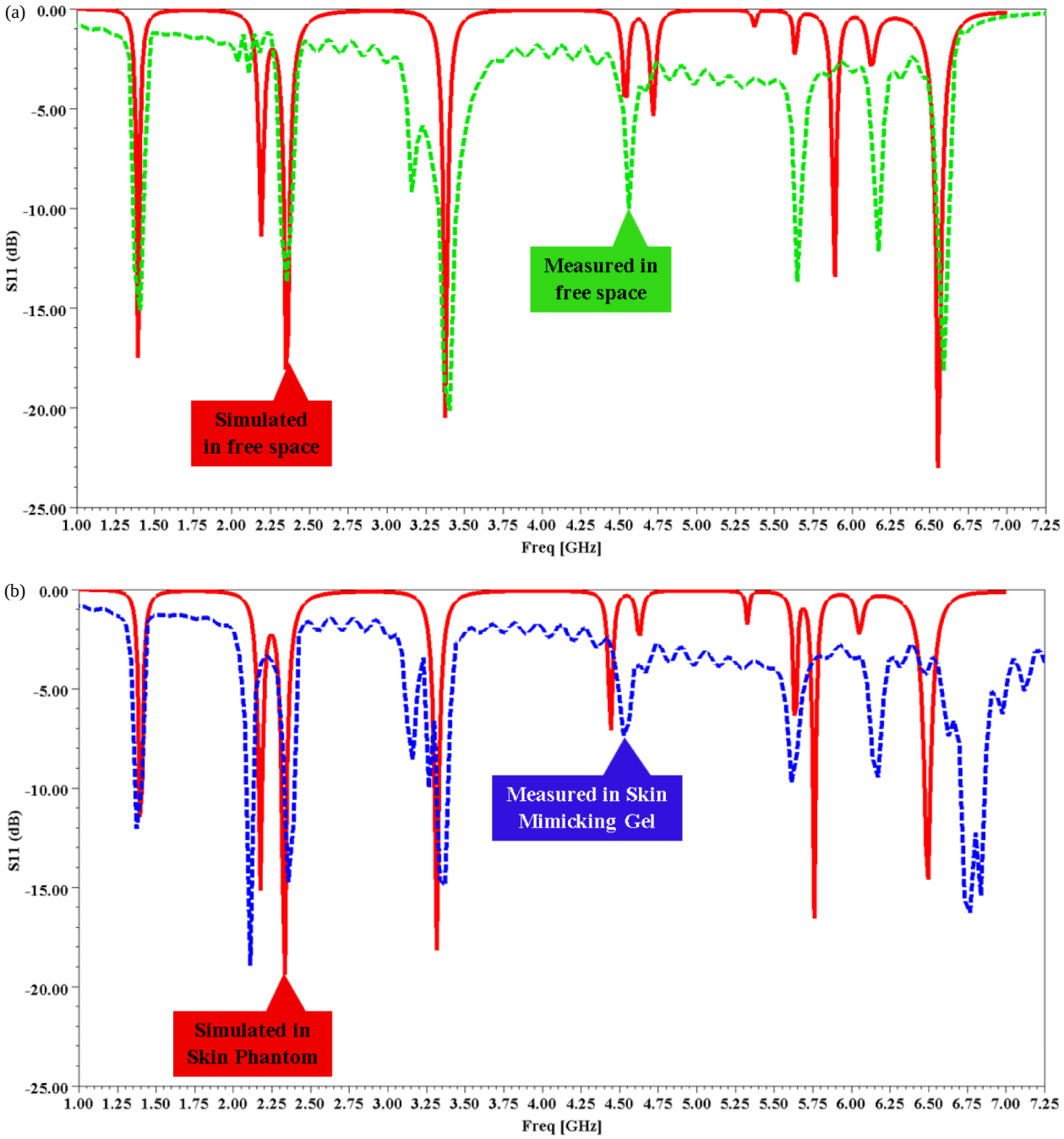

FIGURE 12. Comparison of S_{11} results of proposed antenna in (a) Free space, (b) Human skin.

suggests that the device or system may be better at blocking undesirable signals in these regulatory bands in real life.

6. RESULTS AND DISCUSSION

The tiny circular patch antenna that was presented was studied throughout numerous design iterations (Antenna 1–6) in order to maximize multiband performance while preserving compactness that was acceptable for implanted medical devices. The return loss (S_{11}) graphs indicated that the system operated normally within the designated WMTS, MBAN, and UWB ranges. A three-layer skin phantom (skin, fat, and muscle) showed that the device met IEEE safety standards with a maximum SAR of 0.423 W/kg over 1 g of tissue in the skin layer. Despite the intrinsic losses that occur in biological tissues, gain analysis revealed that the performance was satisfactory. The fat layer exhibited the largest positive gain (0.8 dB), but the overall performance was satisfactory. The mechanical flexibility of the device was confirmed for implantation in non-rigid tissues by bending tests conducted at radii of 100 mm, 130 mm, and 160 mm. These tests revealed low frequency drift and insignificant deterioration at the bandwidth level. When the antenna is subjected to bending situations, the MBAN band exhibited outstanding stability; nevertheless, small fluctuations

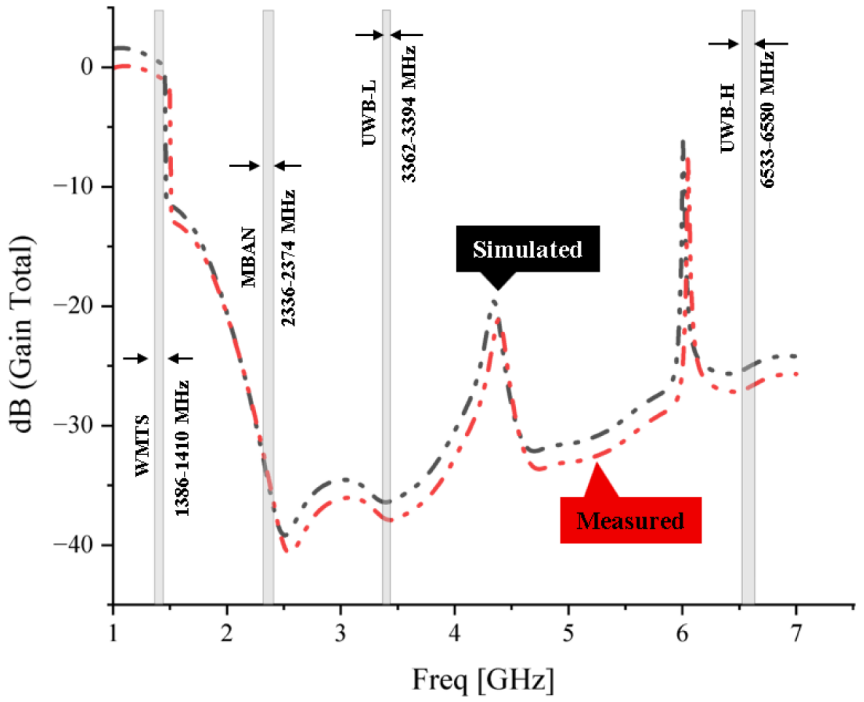

FIGURE 13. Gain comparison of proposed antenna.

were noted in the WMTS and low UWB bands. The structural changes, such as optimal slot arrangement and feed orientation, were found to greatly boost bandwidth without compromising compactness, according to a comparative examination of all of the different variants of the antenna. Miniaturization was made easier by the Rogers RT/Duroid 6010 substrate, which maintained its efficiency while having a high dielectric constant. Multiband capabilities, low SAR, and stable performance under deformation are some of the characteristics that the suggested antenna possesses, which allow it to fulfil the severe criteria for biomedical telemetry. Because of these properties, it is a prospective option for implanted medical devices of the next generation that require a dependable wireless connection.

7. CONCLUSION

A circular patch antenna on a Rogers RT/Duroid 6010/6010LMTM substrate is designed and analyzed in this work. The antenna's diminutive structure, including a ground plane height of 1.27 mm and a metal thickness of 0.035 mm, holds significant potential for high-frequency applications, including biotelemetry and Internet of Medical Things (IoMT) devices. In applications with spatial constraints, the Rogers substrate's high dielectric constant (10.2) facilitates significant miniaturisation while maintaining antenna performance. The substrate supports the resonant cavity necessary for optimal radiation, while a thin, conductive ground plane ensures superior impedance matching and minimises signal losses. The use of slots and disturbances, together with the symmetry of the circular shape, enhances polarisation performance, bandwidth, and radiation efficiency. The device may be made considerably smaller without impacting how it works by using a high-permittivity substrate. The antenna lets you operate with more than one frequency band (WMTS, MBAN, UWB), which is particularly crucial for modern biological telemetry. The design meets safety regulations, and the SAR levels are substantially below what is allowed by IEEE/ICNIRP/FCC limits in all tissue layers. The antenna can bend a lot without breaking; therefore, it can be used in both wearable and internal devices. Compared to most older designs, the antenna has superior gain and efficiency in the provided frequency bands, both in terms of size and performance. Because of the reasons above, the recommended antenna is a suitable solution for next-generation implantable medical devices that need a reliable wireless communication. This circular patch antenna balances compactness and performance in accordance with the growing demand for small, efficient wireless antennas. Future study should focus on enhancing bandwidth further by multilayer patch designs or faulty ground structures, hence facilitating this design for next-generation communication technologies.

REFERENCES

[1] Bao, Z., Y.-X. Guo, and R. Mittra, "Single-layer dual-/tri-band inverted-F antennas for conformal capsule type of applications," *IEEE Transactions on Antennas and Propagation*, Vol. 65, No. 12, 7257–7265, Dec. 2017.

[2] Ganeshwaran, N., J. K. Jeyaprakash, M. G. N. Alsath, and V. Sathyanarayanan, "Design of a dual-band circular implantable antenna for biomedical applications," *IEEE Antennas and Wireless Propagation Letters*, Vol. 19, No. 1, 119–123, 2020.

[3] Liu, Y., Y. Chen, H. Lin, and F. H. Juwono, "A novel differentially fed compact dual-band implantable antenna for biotelemetry applications," *IEEE Antennas and Wireless Propagation Let-*

ters, Vol. 15, 1791–1794, 2016.

[4] Basir, A., M. Zada, Y. Cho, and H. Yoo, "A dual-circular-polarized endoscopic antenna with wideband characteristics and wireless biotelemetric link characterization," *IEEE Transactions on Antennas and Propagation*, Vol. 68, No. 10, 6953–6963, 2020.

[5] Ung, J. and T. Karacolak, "A dual-band meandered dipole antenna for medical telemetry applications," *Progress In Electromagnetics Research C*, Vol. 63, 85–94, 2016.

[6] Gupta, H. K., P. K. Singhal, P. K. Sharma, and V. S. Jadon, "Slotted circular microstrip patch antenna designs for multiband application in wireless communication," *International Journal of Engineering and Technology*, Vol. 1, No. 3, 158–167, 2012.

[7] Sahoo, A. B., G. P. Mishra, and B. B. Mangaraj, "A novel dual slot circular patch antenna design for multi-band applications," *Microwave Review*, Vol. 24, No. 2, 2018.

[8] Remya, V. R., M. Abraham, A. R. Parvathy, and T. Mathew, "Multiband circularly polarised microstrip patch antenna with Minkowski fractal slot for wireless communications," *Progress In Electromagnetics Research C*, Vol. 116, 65–80, 2021.

[9] Kabir, S. S., M. H. Khan, and S. I. Latif, "A multi-band circularly polarized-shared aperture antenna for space applications at S and X bands," *Electronics*, Vol. 12, No. 21, 4439, Oct. 2023.

[10] Singh, D. K., B. Kanaujia, S. Dwari, G. P. Pandey, and S. Kumar, "Multiband circularly polarized stacked microstrip antenna," *Progress In Electromagnetics Research C*, Vol. 56, 55–64, 2015.

[11] Pathak, R., B. B. Mangaraj, A. Kumar, and S. Kumar, "Dual feed multiband microstrip patch antenna design with circular polarized wave for 5G cellular communication," *Progress In Electromagnetics Research B*, Vol. 93, 87–109, 2021.

[12] Shaw, M., B. Deb, and N. Mandal, "Circular Microstrip Patch Antenna with U-slots for multi band application," in *2018 2nd International Conference on Electronics, Materials Engineering & Nano-Technology (IEMENTech)*, 1–3, Kolkata, India, 2018.

[13] Deshmukh, A. A., K. P. Ray, T. Sonwadkar, S. Varawalla, and R. Kataria, "Formulation of resonance frequency for multiband circular microstrip antennas," *International Journal of Microwave and Optical Technology*, Vol. 5, No. 5, 248–256, 2010.

[14] Bhatia, S. S. and J. S. Sivia, "Analysis and design of circular fractal antenna array for multiband applications," *International Journal of Information Technology*, Vol. 14, No. 1, 243–253, 2022.

[15] Wei, K., J.-Y. Li, L. Wang, Z. Xing, and R. Xu, "Study of multiband circularly polarized microstrip antenna with compact size," *Progress In Electromagnetics Research C*, Vol. 58, 11–19, 2015.

[16] Gupta, S. K., A. Sharma, B. K. Kanaujia, S. Rudra, R. R. Mishra, and G. P. Pandey, "Orthogonal slit cut stacked circular patch microstrip antenna for multiband operations," *Microwave and Optical Technology Letters*, Vol. 55, No. 4, 873–882, 2013.

[17] Kardile, V., P. Yadav, and A. Mishra, "Design of multiband circular microstrip patch antenna," *International Research Journal of Engineering and Technology (IRJET)*, Vol. 3, 1961–1963, 2016.

[18] Hu, Z., W. Xin, Y. Luo, Y. Hu, and Y. Zhou, "Design of a modified circular-cut multiband fractal antenna," *The Journal of China Universities of Posts and Telecommunications*, Vol. 23, No. 6, 68–75, Dec. 2016.

[19] Mazen, K., A. Emran, A. S. Shalaby, and A. Yahya, "Design of multi-band microstrip patch antennas for mid-band 5G wireless communication," *International Journal of Advanced Computer Science and Applications (IJACSA)*, Vol. 12, No. 5, 2021.

[20] Singh, A. K., M. P. Abegaonkar, and S. K. Koul, "Miniaturized multiband microstrip patch antenna using metamaterial loading for wireless application," *Progress In Electromagnetics Research C*, Vol. 83, 71–82, 2018.

[21] Jaiswal, A., R. K. Sarin, B. Raj, and S. Sukhija, "A novel circular slotted microstrip-fed patch antenna with three triangle shape defected ground structure for multiband applications," *Advanced Electromagnetics*, Vol. 7, No. 3, 56–63, 2018.

[22] Balanis, C. A., *Antenna Theory: Analysis and Design*, John Wiley & Sons, 2016.

[23] El Atrash, M., M. A. Abdalla, and H. M. Elhennawy, "A wearable dual-band low profile high gain low SAR antenna AMC-backed for WBAN applications," *IEEE Transactions on Antennas and Propagation*, Vol. 67, No. 10, 6378–6388, Oct. 2019.

[24] Green, R. B., M. V. Smith, and E. Topsakal, *In Vitro and In Vivo Testing of Implantable Antennas*, 2021.